Effect of Apical Defects and Doped Atoms on Field Emission of Boron Nitride Nanocones

Wei An, Xiaojun Wu, and X. C. Zeng*

Department of Chemistry and Nebraska Center for Materials and Nanoscience, University of Nebraska−Lincoln, Lincoln, Nebraska 68588

Received: June 1, 2006; In Final Form: June 30, 2006

We present a systematic study of field-emission performance of prototype boron nitride (BN) nanocones using all-electron density-functional theory method. The effects of apical defects and doping/adsorption on the field emission have been evaluated on the basis of magnitude of ionization potential (IP) and electron affinity (EA). Among BN nanocones examined, two 120°-BN nanocones, namely 120°-4-B-N and 120°-55-mol-B, have been identified as promising candidates for the field-emission electron source. Effects of the applied electric field on the electronic structures of BN nanocones have been investigated. In general, the electronic structures of BN nanocones can be significantly modified by a strong electric field, such as the reduction of the HOMO−LUMO gap and the change in density of states. The interaction between BN nanocones and applied electric field can be described by the second-order Stark effect. In addition, calculations show that the doping/adsorption of an impurity atom results in higher IP or EA values, which is unfavorable to the field emission. Our study suggests that BN nanocones can be considered as alternative cold-emission electron sources.

1. Introduction

Nanotubes are promising field-emission electron sources in devices such as flat-panel displays and electron microscopes.[1−6] Unlike conventional thermionic-emission-based cathodes in which thermal potential is the driving force to emit electrons from the cathodes into vacuum, nanotube-based field-emission cathodes that are under a strong external electric field can emit electrons through the energy barrier (via quantum tunneling) between the tip of nanotube and vacuum even at low temperature (cold emission). It is known that material construction and geometric design of the cathodes are the two key factors to affect electron emission, as regulated by Fowler−Nordheim theory.[7,8] Since the nanotube-based emission depends critically on the tip geometry, a commonly used fabrication strategy is to enhance local electric field by using a high aspect ratio of tip. Moreover, in the nanostructure-based field emission, because electrons stem from the discrete energy states of nanostructures, the field-emission performance can be improved if the electronic properties of nanocathodes can be tuned to the desired value of energy gap, Fermi level, and density of states (DOS).

Carbon nanotubes (CNTs) have been studied as cold field-emission electron sources by many researchers.[1−4] However, in production, mixtures of semiconducting and metallic CNTs are commonly attained with the synthesis techniques to date. Unlike CNTs, whose electronic properties are strongly dependent on the chirality and tube diameter,[9] boron nitride nanotubes (BNNTs) exhibit a nearly constant band gap of ca. 5.5 eV with semiconducting properties nearly independent of chirality, tube diameter, and morphology.[10] Also, because of their chemical oxidation inertness and mechanical toughness,[11,12] BN nanostructures are technically even more appealing than CNTs as potential field-emission electron sources.[5] As a novel form of BN nanostructures, BN nanocones hold more promise as field-emission electron sources due to their geometric dependence on the topological defect located at the apex. The conical structure of BN nanocones can be characterized by the disclination angle D_θ, defined as the angle of the sector removed from a flat sheet to form a cone. For graphite-derived carbon nanocones, only five disclination angles ($D_\theta = 60°$, 120°, 180°, 240°, and 300°) are conceivable to meet the continuity condition at the junction of the flat graphite sheet.[13] Unlike the C−C bonds in carbon nanostructures, the isoelectronic BN nanocones consist of three types of covalent bonds, namely, B−N, B−B, and N−N bonds, which contribute differences in physical, chemical, and electronic properties between carbon and boron nitride nanostructures,[14−17] although frustration energy can arise from unfavorable B−B and N−N bond formations.[18−20] To date, BN nanocones with disclination angles of 120°, 240°, and 300° have been synthesized in laboratories.[16,17] In addition, the field-emission current from BNNTs has been experimentally observed at surprisingly low voltage.[5] Hence, it is timely to evaluate electronic properties of BN nanocones under field-emission conditions. In this work, we employed density-functional theory to compute electronic properties that are relevant to the field-emission performance of prototype BN nanocones, as well as to examine the effect of doping/adsorption on these properties. Here, the field-emission performance is evaluated on the basis of the magnitude of ionization potential (IP) and electron affinity (EA) of the BN nanocones subject to a uniform electric field. Effects of the applied electric field on the electronic structures of BN nanocones are also investigated.

2. Models and Computational Methods

The ab initio calculations were performed using the all-electron density-functional theory (DFT) method with the Perdew−Burke−Ernzerhof (PBE) functional[21] implemented in Dmol3 package developed by Accelrys Inc.[22] In Dmol3, the electronic wave function is expanded by using localized atom-centered basis sets in which each basis function is generated numerically on a dense radial grid. In this work, the double

* Corresponding author. E-mail: xczeng@phase2.unl.edu.

10.1021/jp063407k CCC: $33.50
Published on Web 08/05/2006

numerical polarized (DND) basis set is adopted. This basis set is equivalent to the commonly used Pople-type 6-31G(d) basis set. A standard value of 5.5 Å is selected as the basis-set cutoff radius. The structural optimizations were performed to minimize the force on all atoms to be less than 4×10^{-3} au. The self-consistent-field convergence tolerance is set to be 10^{-5} au.

A four-layer BN nanocone system was used, and the nanocone has one of four possible disclination angles, i.e., $D_\theta = 60°$, 120°, 240°, or 300°. The bottom layer of the nanocones was saturated with hydrogen atoms to avoid effects of the dangling bonds on the electronic properties of the finite-size nanocones. Our test calculations showed that the dangling bonds could significantly reduce the highest occupied molecular orbital (HOMO)−lowest unoccupied molecular orbital (LUMO) gap of the BN nanocones.

First, all nanocone structures were fully optimized without symmetry constraint. Next, the optimized structures with the positions of bottom-layer hydrogen, boron, and/or nitrogen atoms fixed were further relaxed in a uniform electric field of 1 V/Å. The field was directed parallel with the central axis of the cone, from tip to the bottom. Note that the length of realistic nanocones typically ranges from 500 nm to 1 μm,[16] and the strong electric field of 1 V/Å is only applicable to the region near the tip of nanocones.[23] Here, we constrained the bottom-layer atoms in the second-stage optimization. This computation strategy is an attempt to focus on the near-tip region and yet to mimic the structural integrity of a long realistic nanocone. The ionization potential (IP) and electron affinity (EA) of each nanocone in the presence of the strong electric field (1 V/Å) were calculated based on the optimized geometry in the second stage. Because of nearly instantaneous tunneling of electrons from the nanocone under a sufficiently high voltage, the structures with positive (+1) or negative (−1) charge are assumed to remain frozen at the neutral geometry. The electrostatic dipole moments, the atomic charges, and the electronic density of states (DOS) were calculated under the emission conditions.

Besides the pristine BN nanocones, we also examined effects of dopants on the electronic properties of BN nanocones. For the BN nanocones with lowest IP and EA values, several types of elemental dopant, which are likely involved in the synthesis process, were studied. Our focus was mainly placed on the effect of apical defects on the IP and EA values. For simplicity, only one dopant atom located on the tip was considered. The optimization procedures were the same as for the pristine BN nanocones, except that the spin-unrestricted calculations were performed for the BN nanocones with dopant, and that all-electron relativistic DFT was used for the third-row heavy transition metal dopant. The bottom-layer constraint was enforced during the geometry optimizations as in the case of pristine BN nanocones. Finally, the system-size effect on the calculated properties was examined.

3. Results and Discussion

3.1. Geometry and Stark Effect. Figure 1 displays the optimized structures of BN nanocones with four different disclination angles and various apical defects. Considering the diversity of disclination angle and defect, we label a BN nanocone structure by using a naming sequence of disclination angle-type/number of ring at the tip-type of antiphase boundary-atoms of apical defect (molecular formula and symmetry in parentheses). Two kinds of antiphase boundaries may exist during the growth process of BN nanocones: (1) a series of parallel B−B or N−N bonds (denoted as mol-B or mol-N) and (2) zigzag types (zig-B or zig-N).[14−16] Both antiphase boundaries are line defects in the BN nanocones.

Figure 2 shows the energy shift of BN nanocones due to the applied electric field (1 V/Å) versus the induced dipole moment. The dipole moments (with and without the applied electric field) were calculated with the bottom-layer hydrogen atoms removed to exclude contributions from the hydrogen. A nearly linear correlation between the energy shift and the induced dipole moment can be seen, indicating that the energy shift (decrease) stems mainly from the electrostatic interaction between the induced dipole and the applied electric field. The geometry optimization (nuclear rearrangement) appears to play a lesser role in the energy shift. Indeed, the geometry change due to the applied electric field is negligible. It is known that the Stark effect describes splitting of energy levels by an external electric field. The Stark effect on 120°-4-B-N and 120°-55-mol-B nanocones can be clearly seen in Figure 3. The energy shift can be well fitted by a quadratic function of the applied field (E_F), that is, $\Delta E = -3.8514E_F^2 - 1.3766E_F - 0.0014$ for 120°-4-B-N and $\Delta E = -4.7543E_F^2 - 1.5417E_F - 0.0023$ for 120°-55-mol-B. The quadratic function signifies the second-order Stark effect. A similar second-order Stark effect is expected for other BN nanocones (see Figure 2).

3.2. Field-Emission Indicators and Electronic Properties. We follow a previous study[23] to utilize the IP value as a field-emission indicator. For semiconductors and insulators with wide band gaps, the EA has also been used as another field-emission indicator.[5] We are aware of that a full description of the field-emission performance is not simple since the electron-emission mechanism is highly dependent on the electronic properties of the material and the shape of the specific cathode. In fact, the electric field near the tip is greatly enhanced relative to the average electric field between the electrodes. The strong local electric field near the tip is neither uniform nor unidirectional but rather converges radially toward the tip. Simulating this highly concentrated local electric field is beyond the scope of this work and possibly impractical. Here, we simply employ a finite-size model system (in a uniform electric field) to mimic the tip of long realistic nanocones under the emission condition described in section 2. The extent to which this simple model system and the uniform-field approximation are applicable requires further investigation and direct comparison with experiments.

Theoretically, the ionization potential (IP) is defined as the energy difference between the cationic system (+1 charge) and the neutral one, while the electron affinity (EA) is defined as the energy difference between the neutral system and the anionic one (−1 charge). In principle, the lower the IP or EA, the easier for an electron to be extracted from the emitter, and the higher field-emission current or lower threshold voltage that can be attained at a given operating voltage. The calculated IPs and EAs for the BN nanocones are given in Table 1. Note that the 120°-55-mol-B and 300°-mol-B nanocones exhibit the lowest and highest IP values, 6.34 and 8.46 eV, respectively; that is, the IP is strongly dependent on the disclination angle. However, there is no obvious correlation between the IP and the disclination angle since there exists more than one type of apical defect for a given disclination angle. As an example, 120°-55-mol-N nanocone has the same IP (6.41 eV) as 60°-5-zig-B, whereas 120°-4-B-N has almost the same IP as 60°-5-mol-B (6.66 and 6.64 eV, respectively); both IP values are larger than those of 120°-55 and 60°-5-zig-B nanocones. Based on the IP indicator, it seems that the 120°-55-mol-B nanocone is the best candidate for a field-emission electron source. The 60°-5-zig-B

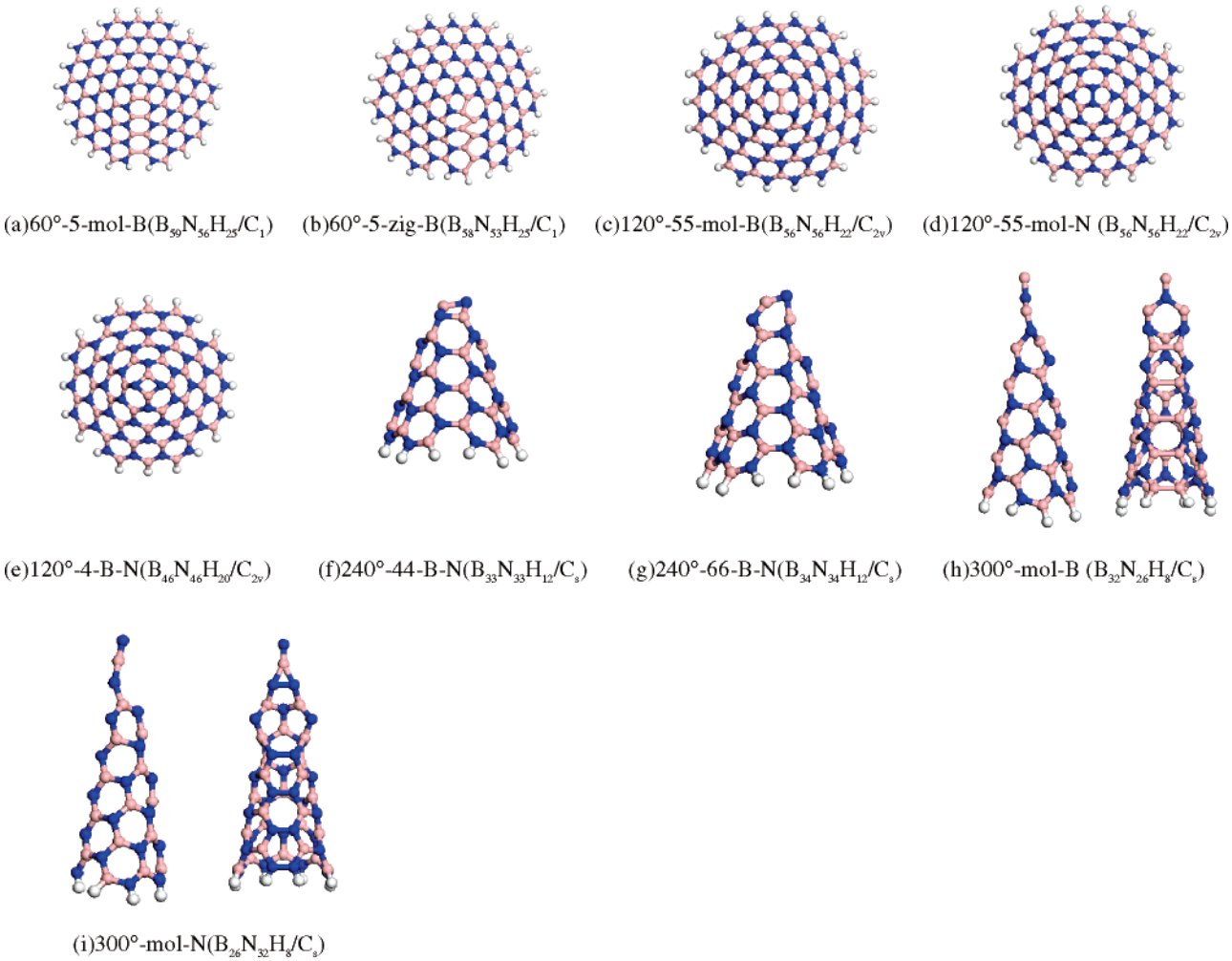

Figure 1. Optimized structures of BN nanocones with four different disclination angles and various apical defects. The labels are defined in the text. B, N, and H atoms are colored in reddish yellow, blue, and white, respectively. Two side views by 90° rotation about the cone axis are displayed in (h) and (i).

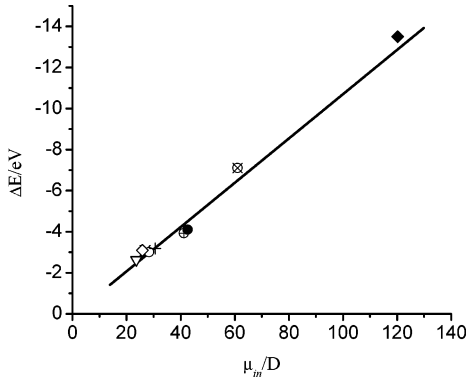

Figure 2. Energy shift of BN nanocones versus induced dipole moment, due to applied electric field (1 V/Å). Symbol designations for the nanocone models shown in Figure 1. (a) ×; (b) ▽; (c) ●; (d) +; (e) ○; (f) ⊕; (g) ⊗; (h) ◆; (i) ◇.

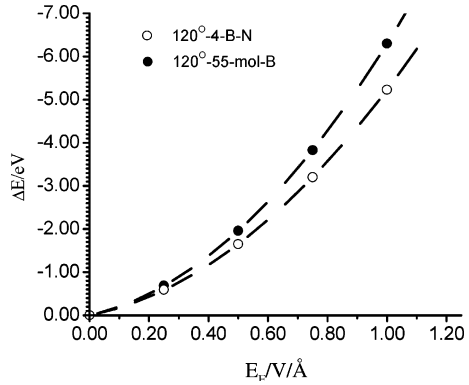

Figure 3. Energy shift of 120°-4-B-N (○) and 120°-55-mol-B (●) nanocones versus strength of applied electric field.

and 120°-55-mol-N nanocones could also be promising candidates because their IP values are merely 0.07 eV larger than that of the 120°-55-mol-B nanocone. This conclusion bears some similarity to that in the case of BNNTs, namely, the IP of B-terminated zigzag BNNT is smaller than that of N-terminated BNNT.[24]

On the other hand, the EA indicator suggests a different best candidate, namely, 120°-4-B-N (EA 1.25 eV). Field emission can be related to a negative electron affinity (NEA) when the minimum energy of electrons in the conduction band lies above the vacuum energy level. As such, any electrons promoted into the conduction band could escape from the emitter surface into the vacuum. Both c-BN and h-BN bulk materials have been shown to exhibit NEA surface behavior.[25] Under a strong electric field, the induced charges emerge at the tip due to the high aspect ratio of the nanocone (see Figure 4). As a result, the nanocone emitter is polarized and thus carries net negative charge at the tip when connected to an electron reservoir at the

TABLE 1: Ionization Potential (IP) and Electron Affinity (EA) of BN Nanocones with Four Different Disclination Angles and Various Apical Defects with Applied Electric Field of 1 V/Å[a]

BN nanocones	IP (eV)	EA (eV)
60°-5-mol-B	6.64	1.78
60°-5-zig-B	6.41	2.43
120°-55-mol-B	**6.34**	2.60
120°-55-mol-N	6.41	1.35
120°-4-B-N	6.66	**1.25**
240°-44-B-N	6.95	2.50
240°-66-B-N	7.00	5.04
300°-mol-B	8.46	6.02
300°-mol-N	8.40	5.81

[a] The boldface values denote the lowest IP and EA values.

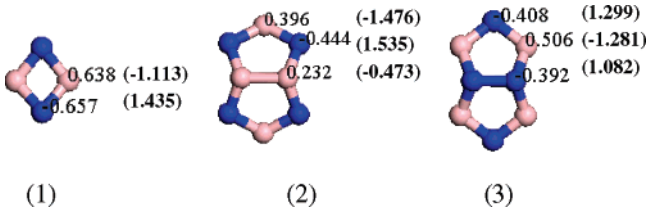

Figure 4. Electric-static-potential-fitted charges at the tip of (1) 120°-4-B-N, (2) 120°-55-mol-B, and (3) 120°-55-mol-N nanocones with (in boldface) and without applied electric field (1 V/Å).

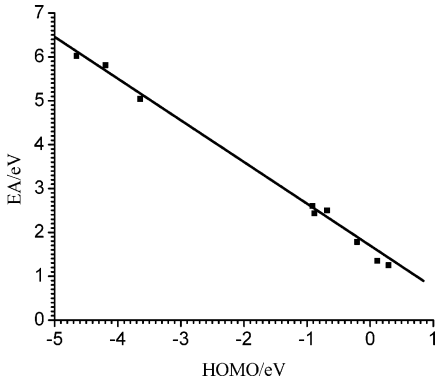

Figure 5. EAs of BN nanocones versus corresponding HOMO levels. The applied electric field is 1 V/Å.

threshold of electron tunneling.[26] Similar to IPs, the calculated EAs are also strongly dependent on the disclination angle and apical defects. For example, at the disclination angle of 120°, 4-B-N, 55-mol-N, and 55-mol-B exhibit an EA value of 1.25, 1.35, and 2.60 eV, respectively. However, at the disclination angle of 240°, 44-B-N and 66-B-N exhibit an EA value of 2.50 and 5.04 eV, respectively. There is linear correlation between EAs and the corresponding HOMOs of negatively charged BN nanocones, as shown in Figure 5.

The insight into electronic structures of emitters at the threshold of electron emission can be useful for understanding field-emission quantum effect and for developing more efficient electron sources. Figure 6 shows the DOS of BN nanocones under different conditions. Note that all plots are made with the same energy and density scale, without overlapping the Fermi level. It can be seen that all BN nanocones are semiconducting with finite energy gaps between occupied and empty electronic states in the zero electric field (dotted line). Both 300°-mol-B and 300°-mol-N nanocones have the smallest energy gap, while 120°-4-B-N, 120°-55-mol-B, and 120°-55-mol-N have the largest energy gap. The energy gaps appear to be dependent on not only disclination angles[16] but also apical

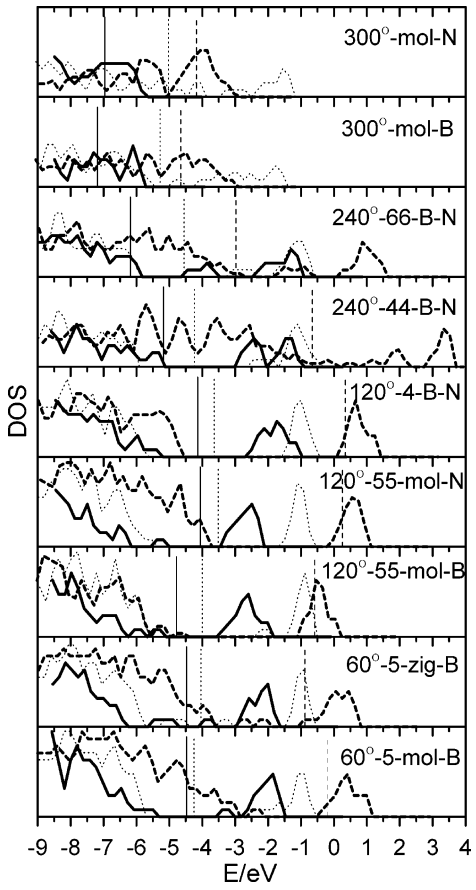

Figure 6. Density of states (DOS) of neutral (dotted and solid lines) and negatively charged (dashed line) BN nanocones with (solid and dashed lines) and without (dotted line) applied electric field (1 V/Å). Vertical lines denote the corresponding Fermi level in each case (dotted, solid, and dashed lines).

defects. For example, 60°-5-mol-B and 60°-5-zig-B have 3.39 and 1.40 eV of HOMO−LUMO gap, respectively; 120°-55-mol-B, 120°-55-mol-N, and 120°-4-B-N have 3.68, 4.30, and 4.67 eV of energy gap, respectively; and 300°-mol-B and 300°-mol-N have 0.85 and 0.11 eV, respectively (see Table S1). Although having the smallest energy gap, neither 300°-mol-B nor 300°-mol-N is good for field-emission purposes, due to their relatively high IP and EA values.

With the applied electric field (1 V/Å), the energy gap is reduced and the Fermi level (chemical potential) is lowered. Due to the electrostatic interaction between the induced dipole and the applied electric field, the nanocones become more energetically stable, a manifestation of the Stark effect (Figures 2 and 3). For BN nanocones with negative charge (−1), the energy gaps are appreciably reduced and can even become zero while their Fermi levels are shifted up, particularly for 120°-4-B-N, 120°-55-mol-N, and 120°-55-mol-B, whose Fermi levels are close to or even above 0 eV (vacuum). The densest occupancy of electronic states near the Fermi level is also evident for negatively charged 120°-4-B-N, 120°-55-mol-N, and 120°-55-mol-B. The HOMO−LUMO gaps of 120°-4-B-N and 120°-55-mol-B decrease linearly with increasing field as shown in Figure 7, demonstrating the strong effect of electric field on the electronic structure of BN nanocones.

The emission electrons can emanate from either a neutral or negatively charged emitter at the threshold of emission. If a BN nanocone emitter is neutral, the applied electric field generally reduces its energy gap and lowers the Fermi level

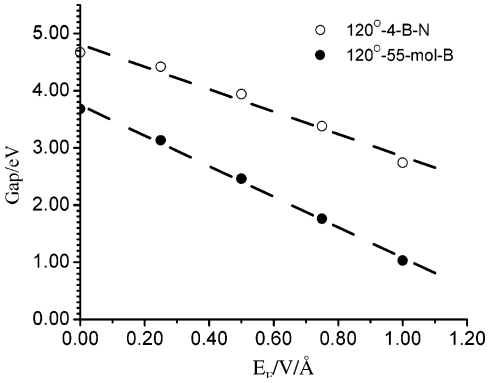

Figure 7. Effect of electric field on HOMO−LUMO gap of 120°-4-B-N (○) and 120°-55-mol-B (●) nanocones.

because of the second-order Stark effect. A reduction of IP with increasing field (Table S2) supports the use of IP as a field-emission indicator. Indeed, the emission-current density is greatly enhanced with increasing the field, according to Fowler−Nordheim equation.[7,8] If a BN nanocone emitter is negatively charged, the EA can be used as a field-emission indicator. The EAs increase with increasing field (Table S2), suggesting that the BN nanocones can be negatively charged more easily with the stronger field. The net negative charge trapped by defects of a BN nanocone can be in a bound electronic state and serve as emission electrons at the threshold of emission.

Figure 8 shows the electron-density isosurfaces of the HOMO for negatively charged 120°-4-B-N, 120°-55-mol-B, and 120°-55-mol-N, respectively, with the applied electric field (1 V/Å). Clearly, the HOMO electronic density is highly confined near the tip region and localized prominently at B atoms. The latter is consistent with the negative charge transfer from N to B atoms due to the applied electric field (see Figure 4). Moreover, atomic sites around the tip of the 120° BN nanocones have the maximum surface electrostatic potential, mostly around B atoms rather than N atoms, as shown in Figure 9, suggesting that the electrons most likely emit from B atoms near the tip. This unique feature of field emission can be attributed to the structural anomalies[27] of the BN nanocones, such as the formation of B−B and N−N bonds, as well as the existence of a four-member ring at the apex of the 120° BN nanocones. Note again that the B−B and N−N bonds are energetically unfavorable compared to normal B−N bonds. However, they are likely to survive the nonequilibrium microscopic growth of BN nanostructures or to be generated by outside perturbations[19,20,28] for which Stone-Walls defects are an example.[28a,b]

We thus propose an electron-emission mechanism for the BN nanocone emitter. The electrons (or net negative charges) near the tip may tunnel through a triangle-shape-like energy barrier into the vacuum, a result of enhanced local field near the tip. A strong field may turn a semiconducting BN nanocone into a metallic-like one such that electrons may transport ballistically, from the sidewall to the tip, when connected to an electron reservoir. The mechanism proposed here does not include electron transportation between the electron reservoir (metal substrate) and the BN nanocone sidewall. Note also that those BN nanocones which show metallic-like electronic structure (in applied field), such as 240°-66-B-N, 300°-mol-B, and 300°-mol-N, are not directly related to the field-emission capability (see Table 1, Table S1, and Figure 6).

3.3. Doping/Adsorption Effect on Field Emission. In reality, pristine BN nanocones may be doped with impurity atoms during the synthesis process. For instance, W and Hf are used as electrodes in the arc discharge process; Co and Ni are used as catalysts in the laser ablation process; oxides of Mo, Cu, and Au are used as promoters when CNTs are involved as templates; Fe, Zn, Mg, Na, and Li are used as catalysts in chemical vapor deposition (see ref 12 and references therein). Moreover, Pt has been used to modify BNNTs to enhance hydrogen storage.[29] For BN nanocones, metallic particles have been observed to be encapsulated near the tip.[12] Therefore, it is interesting to see the effect of doped or adsorbed metal atoms on the filed-emission capability of BN nanocones.

We used the 120°-55-mol-B and 120°-4-B-N model systems to test the doping/adsorption effect. For simplicity, we only considered one metal atom located at the apical defect because the defect site experiences more strain[28] and is likely to be chemically more reactive than the perfect sidewall.[30] The binding energy of a single metal atom to the nanocone sidewall is given by BE $= E_{\text{cone+doped atom}} - E_{\text{cone}} - E_{\text{doped atom}}$. The negative (positive) BE denotes an exothermic (endothermic) process. Scalar relativitistic DFT was used to calculate binding energies of the third-row transition atoms Hf, W, Pt, and Au with the BN nanocones.

For the doped 120°-55-mol-B nanocone, a wide range of negative binding energy is obtained, ranging from −3.3 to −118.6 kcal/mol (Table 2). However, only carbon and transition metals with unfilled d orbitals can withstand the applied electric field of 1 V/Å without being desorbed from the tip (see Figure S1). Other dopants cannot bind with the nanocones in such a strong electric field. For the 120°-4-B-N nanocone, the binding energies (Table S3) are much smaller compared to those with the 120°-55-mol-B counterparts, indicating that the B−N bond of the four-member ring is chemically less reactive than the B−B bond. It is noteworthy that as the atomic number of transition metals increases from Fe to Zn, the variation of BEs follows the same trend as the variation of coordinate−covalent bonding energy of the 3d transition metal−ligand complexes. In the metal−ligand complexes, the crystal-field stabilization energies in the weak field situation increase from Fe ($t_{2g}^4e_g^2$) to Ni ($t_{2g}^6e_g^2$) and then decrease from Ni ($t_{2g}^6e_g^2$) to Zn ($t_{2g}^6e_g^4$). Based on the BE values and the bond lengths (Figure S1 and Table S4), carbon and transition-metal elements are essentially covalently bonded (chemisorbed) to the 120°-55-mol-B tip, while Li, Na, Mg, and Zn are physisorbed to the tip through weak van der Waals interactions. Note that DFT tends to underestimate weak van der Waals interactions between dopants and nanotubes.[31] To obtain an accurate binding energy in the case of physisorption, higher level ab initio methods are required as shown in a recent study on weak interactions between metal atoms Li, Ca, and Al and aromatic carbon systems.[32] Therefore, the BEs for physisorption reported in this study only provide a semiquantitative guideline. Almost all dopants considered here (with exception of carbon) are charge donors with partial charge (0.06−0.43*e* per doped atom) transferred to 120°-55-mol-B (Table S5). The charge transfers are correlated to some extent with their IP increase, relative to that of the pristine 120°-55-mol-B nanocone (see Table 3 and Table S5). Overall, the interaction between dopant/adsorbent and the B−N bond of the four-member ring is much weaker than that with the B−B bond; the transition metals interact with the tip more strongly than the metals in main groups. Note also that only the 120°-4-B-N nanocone doped with carbon atom can withstand the strong applied field (1 V/Å). The IPs and EAs of 120°-55-mol-B nanocone with dopant in the applied electric field (1 V/Å) are given in Table 3. Because of the uniformly higher IP and EA values of the nanocones with the dopant, doping/adsorption of impurity atoms is unfavorable for the field-emission purpose.

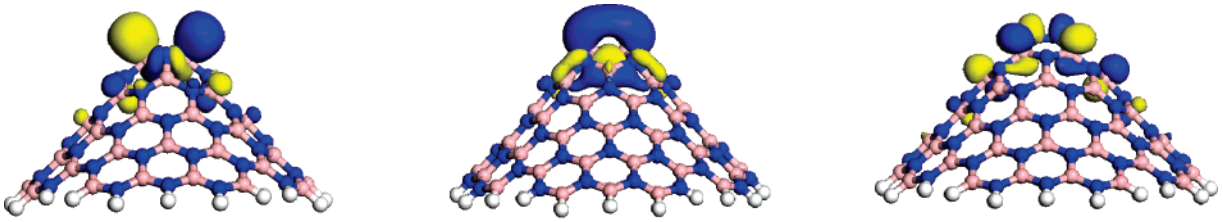

Figure 8. Electron-density isosurfaces of HOMO generated with isovalue of ±0.03 e/Å^3 for negatively charged (1) 120°-4-B-N, (2) 120°-55-mol-B, and (3) 120°-55-mol-N nanocones. The applied electric field is 1 V/Å.

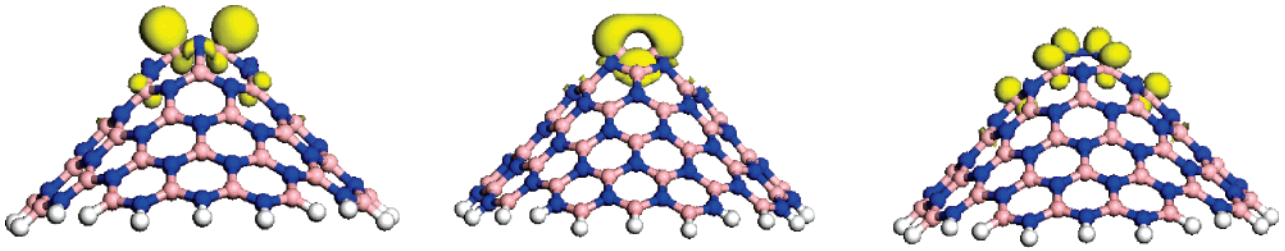

Figure 9. Electrostatic-potential isosurfaces generated with isovalue of ±10 kcal/mol for negatively charged (1) 120°-4-B-N, (2) 120°-55-mol-B, and (3) 120°-55-mol-N nanocones. The applied electric field is 1 V/Å.

TABLE 2: Binding Energy (BE) of 120°-55-mol-B Nanocone with Various Doped/Adsorbed Atoms (in Zero Field)

doped/adsorbed atoms[a]	BE (kcal/mol)	doped/adsorbed atoms	BE (kcal/mol)
Pt	−110.8	Na	−11.6
Fe	−51.7	Li	−17.3
Co	−71.2	Mg	−5.8
Ni	−78.2	Zn	−3.3
Mo	−13.7	Cu	−30.8
W	−90.4	Au	−48.1
Hf	−68.7		
C	−118.6		

[a] The dopants and adsorbents shown in the left column can bind with the BN nanocones even in the strong electric field of 1 V/Å. All geometric structures exhibit C_{2v} symmetry.

TABLE 3: Ionization Potential (IP) and Electron Affinity (EA) of 120°-55-mol-B Nanocone with Various Doped Atoms[a]

doped/adsorbed atoms	IP (eV)	EA (eV)
Pt	6.64	4.66
Fe	6.66	4.50
Co	6.74	4.69
Ni	6.54	4.42
Mo	6.92	4.83
W	6.86	4.75
Hf	6.81	4.73
C	6.48	4.64
C[b]	6.71	2.46

[a] The applied electric field is 1 V/Å. [b] With 120°-4-B-N nanocone.

3.4. System-Size Effect. When a finite model system is used to simulate a realistic long nanocone system, the finite-size effect should be carefully examined. First, we note that the size effect on the electronic structure of BN nanocones is very small in the zero field (Table S6); however, the HOMO−LUMO gaps of 120°-4-B-N and 120°-55-mol-B are reduced more significantly as the model size increases in the nonzero field. The latter result indicates that the large-sized BN nanocones behave more like metals in a strong electric field. Table 4 demonstrates the system-size effect on IPs and EAs for the 120°-4-B-N, 120°-55-mol-B, and 300°-mol-B nanocones in nonzero field. For 120°-4-B-N and 120°-55-mol-B, the IP decreases with the size of system whereas the EAs increase. For 300°-mol-B, EAs increase with the size of the system but IPs change much less than those of 120°-4-B-N and 120°-55-mol-B. Still, based on the IP and EA indicators, the best candidates predicted for field emission remain the same as those described in section 3.3.

TABLE 4: Ionization Potential (IP) and Electron Affinity (EA) of (1) 120°-4-B-N, (2) 120°-55-mol-B, and (3) 300°-mol-B Nanocones with Three Different Sizes of Model System[a]

cones/symmetry	size/formula	IP (eV)	EA (eV)
(1)/C_s	4-layered/$B_{46}N_{46}H_{20}$	6.66	1.25
	6-layered/$B_{94}N_{94}H_{28}$	5.54	2.54
	9-layered/$B_{196}N_{196}H_{40}$	4.76	4.00
(2)/C_{2v}	2-layered/$B_{24}N_{24}H_{14}$	7.31	1.52
	4-layered/$B_{56}N_{56}H_{22}$	6.34	2.60
	6-layered/$B_{112}N_{112}H_{30}$	5.39	3.92
(3)/C_s	3-layered/$B_{19}N_{15}H_6$	8.42	5.50
	5-layered/$B_{32}N_{26}H_8$	8.46	6.02
	7-layered/$B_{51}N_{43}H_{10}$	8.67	6.56

[a] The applied electric field is 1 V/Å.

4. Conclusion

We have performed ab initio calculations to evaluate the field-emission performance of prototype BN nanocones and examined the effect of doping/adsorption on the field emission. The field-emission performance is assessed on the basis of ionization potential (IP) and electron affinity (EA) values. Effects of the applied electric field on the electronic structures of BN nanocones are also investigated. The 120°-4-B-N and 120°-55-mol-B nanocones appear to be two promising candidates for the field-emission electron source. Because of the strong B−N covalent bond, the energy barrier for surface migration of emitter atoms is much higher than that of the metal emitter, thereby

rendering the BN nanocone emitter capable of withstanding an extremely strong electric field without much geometry distortion and heat production. In general, the electronic structure of BN nanocones can be greatly altered by a strong electric field, notably, the reduction of the HOMO−LUMO gap. The interaction between BN nanocones and the applied electric field can be described by the second-order Stark effect. An electron emission mechanism is proposed for semiconduting BN nanocones at the threshold of emission. In addition, our calculations show that the doping/adsorption of an impurity atom generally results in higher IP or EA values, which is not beneficial to the field emission. In summary, because of their unique chemical, electrical, and mechanical properties, as well as excellent flexibility and elasticity,[33] BN nanocones can be considered as alternative cold-emission electron sources, e.g., in single-electron-beam instruments such as electron microscopes, or as applied in high-performance nanoelectronic devices under extreme environments. Indeed, we found that the field-emission efficiency for the best BN nanocones is comparable to the metallic armchair (5,5) CNT emitter because of their comparable IP values (6.4 eV for CNT).[23] We suggest that future experiments could give more attention to the BN nanocones, particularly those with 120° disclination angle, and examine their potential as field-emission electron sources.

Acknowledgment. This research was supported in part by grants from DOE (DE-FG02-04ER46164), NSF (CHE and MRSEC), the John Simon Guggenheim Foundation, and the Nebraska Research Initiative (X.C.Z.), and by the Research Computing Facility at University of Nebraska−Lincoln.

Supporting Information Available: Structures of 120°-55-mol-B with various doped atoms at the tip are presented in Figure S1; IP, EA, BE, charge transfers, and other electronic properties for 120°-4-B-N, 120°-55-mol-B, and 300°-mol-B are presented in Tables S1−S6. This material is available free of charge via the Internet at http://pubs.acs.org.

References and Notes

(1) de Heer, W. A.; Chatelain, A.; Ugarte, D. *Science* **1995**, *270*, 1179.
(2) Baughman, R. H.; Zakhidov, A. A.; de Heer, W. A. *Science* **2002**, *297*, 787.
(3) Fan, S.; Chapline, M. G.; Franklin, N. R.; Tombler, T. W.; Cassell, A. M.; Dai, H. *Science* **1999**, *283*, 512.
(4) Shakir, M. I.; Nadeem, M.; Shahid, S. A.; Mohamed, N. M. *Nanotechnology* **2006**, *17*, 41.
(5) Cumings, J.; Zettl, A. *Solid State Commun.* **2004**, *129*, 661.
(6) Dorozhkin, P.; Golberg, D.; Bando, Y.; Dong, Z. C. *Appl. Phys. Lett.* **2002**, *81*, 1083.
(7) Fowler, R. H.; Nordheim, L. *Proc. R. Soc. A* **1928**, *119*, 173.
(8) Houston, J. M. *Phys. Rev.* **1952**, *88*, 349.
(9) (a) Saito, R.; Fujita, M.; Dresselhaus, G.; Dresselhaus, M. S. *Appl. Phys. Lett.* **1992**, *60*, 2204. (b) Wildöer, J. W. G.; Venema, L. C.; Rinzler, A. G.; Smalley, R. E.; Dekker, C. *Nature* **1998**, *391*, 59.
(10) Blase, X.; Rubio, A.; Louie, S. G.; Cohen, M. L. *Eur. Phys. Lett.* **1994**, *28*, 335.
(11) Chen, Y.; Zou, J.; Campbell, S. J.; Caer, G. Le. *Appl. Phys. Lett.* **2004**, *84*, 2430.
(12) Ma, R. Z.; Golberg, D.; Bando, Y.; Sasaki, T. *Philos. Trans. R. Soc. London, Ser. A* **2004**, *362*, 2161.
(13) Krishnan, A.; Dujardin, E.; Treacy, M. M. J.; Hugdahl, J.; Lynum, S.; Ebbesen, T. W. *Nature* **1997**, *388*, 451.
(14) Azevedo, S.; Mazzoni, M. S. C.; Chacham, H.; Nunes, R. W. *Appl. Phys. Lett.* **2003**, *82*, 2323.
(15) Azevedo, S.; Mazzoni, M. S. C.; Nunes, R. W.; Chacham, H. *Phys. Rev. B* **2004**, *70*, 205412.
(16) Zhi, C.; Bando, Y.; Tang, C.; Golberg, D. *Phys. Rev. B* **2005**, *72*, 245419.
(17) Bourgeois, L.; Bando, Y.; Han, W. Q.; Sato, T. *Phys. Rev. B* **2000**, *61*, 7686.
(18) Charlier; Blase, X.; De Vita, A.; Car, R. *Appl. Phys. A* **1999**, *68*, 267.
(19) Golberg, D.; Bando, Y.; Eremets, M.; Takemura, K.; Kurashima, K.; Yusa, H. *Appl. Phys. Lett.* **1996**, *69*, 2045.
(20) Saito, Y.; Maida, M. *J. Phys. Chem. A* **1999**, *103*, 1291.
(21) (a) Perdew, J. P.; Burke, K.; Ernzerhof, M. *Phys. Rev. Lett.* **1996**, *77*, 3865. (b) Perdew, J. P.; Burke, K.; Ernzerhof, M. *Phys. Rev. Lett.* **1997**, *78*, 1396.
(22) (a) Delley, B. *J. Chem. Phys.* **1990**, *92*, 508. (b) Delley, B. *J. Chem. Phys.* **2000**, *113*, 7756.
(23) Maiti, A.; Andelm, J.; Tanpipat, N.; von Allmen, P. *Phys. Rev. Lett.* **2001**, *87*, 155502.
(24) Hou, S. M.; Shen, Z. Y.; Zhang, J. X.; Zhao, X. G.; Xue, Z. Q. *Chem. Phys. Lett.* **2004**, *393*, 179.
(25) Powers, M. J.; Benjamin, M. C.; Porter, L. M.; Nemanich, R. J.; Davis, R. F. *Appl. Phys. Lett.* **1995**, *67*, 3912.
(26) Luo, J.; Peng, L. M.; Xue, Z. Q.; Wu, J. L.*Phys. Rev. B* **2002**, *66*, 155407.
(27) Geis, M. W.; Efremow, N. N.; Krohn, K. E.; Twichell, J. C.; Lyszczarz, T. M.; Kalish, R.; Greer, J. A.; Tabat, M. D. *Nature* **1998**, *393*, 431.
(28) (a) Bettinger, H. F.; Dumitrica, T.; Scuseria, G. E.; Yakobson, B. I. *Phys. Rev. B* **2002**, *65*, 041406. (b) Miyamoto, Y.; Rubio, A.; Berber, S.; Yoon, M.; Tomanek, D. *Phys. Rev. B* **2004**, *69*, 121413. (c) Schmidt, T. M.; Baierle, R. J.; Piquini, P.; Fazzio, A. *Phys. Rev. B* **2003**, *67*, 113407. (d) Kang, H. S. *J. Phys. Chem. B* **2006**, *110*, 4621.
(29) Tang, C.; Bando, Y.; Ding, X.; Qi, S.; Golberg, D. *J. Am. Chem. Soc.* **2002**, *124*, 14550.
(30) (a) Chakrapani, N.; Zhang, Y. M.; Nayak, S. K.; Moore, J. A.; Carroll, D. L.; Choi, Y. Y.; Ajayan, P. M. *J. Phys. Chem. B* **2003**, *107*, 9308. (b) Picozzi, S.; Santucci, S.; Lozzi, L.; Valentini, L.; Delley, B. *J. Chem. Phys.* **2004**, *120*, 7147.
(31) (a) Jhi, S. H.; Kwon, Y. K. *Phys. Rev. B* **2004**, *69*, 245407. (b) Zhao, J.; Buldum, A.; Han, J.; Lu, J. P. *Nanotechnology* **2002**, *13*, 195.
(32) Zhao, Y. L.; Lin, C. S.; Zhang, R. Q.; Wang, R. S. *J. Chem. Phys.* **2005**, *122*, 194322.
(33) Xu, F. F.; Bando, Y.; Golberg, D.; Ma, R. Z.; Li, Y. B.; Tang, C. C. *J. Chem. Phys.* **2003**, *119*, 3436.